Full Paper

Israel Journal of Chemistry

www.ijc.wiley-vch.de

doi.org/10.1002/ijch.202100082

Substrate Dependent Charge Transfer Kinetics at the Solid/Liquid Interface of Carbon-Based Electrodes with Potential Application for Organic Na-Ion Batteries

Daniel Werner,[a] Thöny Alexander,[a] Daniel Winkler,[a] Dogukan H. Apaydin,[b] Thomas Loerting,[a] and Engelbert Portenkirchner*[a]

Dedicated to the 60th birthdate of Ord. Prof. Mag. Dr. DDr. h.c. Niyazi Serdar Sariciftci

Abstract: Electroactive organic semiconducting pigments represent a group of very promising electrode materials for the next generation of energy conversion and storage technologies. However, most pigments suffer from high solubility in organic electrolytes and poor electrical conductivity, which have severely impeded their practical applications. Among different strategies to improve their electrochemical performance, using conductive carbon substrates to form composite electrodes is one of the most used methods to solve these problems. In this work we investigate the role of conductive carbon substrates towards their charge transfer kinetics at the solid/liquid interface with potential application for organic sodium (Na)-ion batteries. This study reveals that the role of conductive carbon is related not only to the optimal electronic path but also to the ionic path towards the electrode active material. Perylentetracarboxylicdiimide is used as the electrode active material coated on graphite/copper and carbon paper substrates. The morphology, structure, and chemical composition of our electrodes are investigated via scanning electron microscopy, X-ray photoelectron and Raman spectroscopy. A thorough kinetic analysis is systematically implemented by cyclic voltammetry and electrochemical impedance spectroscopy. We performed a quantitative analysis of the resistance and capacitive components of the composite electrodes using the theory of the transmission line model and electrochemical impedance spectroscopy with symmetric cells. Our results indicate that a decrease in pore resistance is key to achieve high charge transfer kinetics in electrochemical systems. This work will therefore contribute towards future, efficient electrode design with low pore resistance and high charge transfer kinetics. This may prove of great importance for the development of energy conversion and storage technologies, including heterojunction solar cells, electrocatalysts/photocatalysts for water splitting, carbon dioxide (CO_2) reduction and lithium (Li)- and Na-ion batteries.

Keywords: charge transfer · carbon electrodes · substrate · organic · Na-ion batteries

1. Introduction

The enormous thirst of humanity for cheap and steadily available energy, in combination with a reckless exploitation of fossil fuels like coal, oil and gas has major impacts on our lives, economy, and society.[1] The combustion of fossil fuels results in environmental pollution, habitat loss, decreasing biodiversity and the emission of carbon dioxide (CO_2), which is considered as the main greenhouse gas.[2,3] In the course of climate change mitigation the development of carbon neutral technologies has become crucial for a sustainable development of our society,[4,5] resulting in a particular interest in studies that advance our knowledge on next-generation energy-related technologies.[6–8]

In search for suitable materials that provide a stable support under various environmental conditions, offer efficient charge transfer kinetics and are economically feasible, carbon and its allotropes (i.e. graphite, hard carbon, glassy carbon) are widely investigated as carrier substrates used in energy conversion and storage technologies.[9–11] Carbon is an extremely interesting element owing to its capability of forming sp^2 (graphite-like) and sp^3 (diamond-like) hybridized chemical bonds in diverse ratios, which is resulting in a rich chemistry and various allotrope forms.[12–14] Recent advances in nano-structuring carbon have further opened new applications of carbon to be used in various energy storage technologies.[15–18] Among a multitude of applications one finds that carbon based nanomaterials are used to overcome

---

[a] *D. Werner, T. Alexander, D. Winkler, T. Loerting, E. Portenkirchner*
Institute of Physical Chemistry, University of Innsbruck, 6020 Innsbruck, Austria
E-mail: Engelbert.Portenkirchner@uibk.ac.at
[b] *D. H. Apaydin*
Institute of Materials Chemistry, TU Wien, 1060 Vienna, Austria

intrinsic limitations in solar cells based on carbon nanomaterials,[19–23] and are heavily used as either active components or supports in electrocatalysis,[24–26] and fuel cells.[27] Carbon materials derived from biomass are widely applied in bioelectrochemical systems,[28–30] biosensing applications,[31] and ITO electrode replacement.[32] Additionally, their high electrical conductivity and overall stability during cycling, makes carbon based materials suitable for rechargeable electrochemical power sources, such as batteries, including stationary and large-scale systems,[10,33,34] supercapacitors,[35,36] Na-ion batteries,[37–39] and Na-ion capacitors.[40] For all these applications, an efficient charge transfer at the materials interfaces (solid/solid or solid/liquid) is crucial and found to be ideal for applications in combination with organic semiconductors (OSCs).

OSCs have been researched and utilized equally in diverse fields like organic solar cells,[41,42] organic field effect transistors,[43] organic light emitting diodes,[44] electrocatalytic[45] and photoelectrocatalytic[46] applications. Stability of OSCs has been the subject of extensive research. Among OSCs, pigments stand out due to their stability against harsh conditions like extreme pH and temperatures. One particular group of pigments, namely, perylene diimides (PDIs) are of specific interest as they can be synthesized in high yields and can be chemically modified at bay positions which offer further functionalization.[47] Their carbonyl groups, which can undergo redox reactions, combined with their unique π-π layer stacking ability, rendered them attractive candidates for battery applications in the last decade.[48] Perylene based batteries offer high theoretical capacities and fast reaction kinetics.[49,50] PDI based batteries have been utilized in various forms such as carboxylates,[48] in polymer form,[49,51] and combined with carbon black.[52] In recent years PDIs have also shown potential to be used in Na-ion batteries.[39,53] Our group has shown that an industrially-relevant pigment, perylene tetracarboxylic diimide (PTCDI, Scheme 1), is capable of delivering high sodiation rates (2.3 A g^{-1}) with a capacity of 78 mAh g^{-1} under 5 minutes charging time.[39]

In this work we investigate the role of two different conductive carbon substrates, graphite/copper (CuC) and carbon paper (Cp), towards their charge transfer kinetics at the solid/solid and solid/liquid interface. Both substrates are widely used for energy conversion and energy storage applications.[37,54–59] We show that the role of conductive carbon is related not only to the optimal electronic path but also to the ionic path towards the electrode active material. The OSC pigment PTCDI is used as the electrode active material. We start by investigating the morphology, structure, and chemical composition of our electrodes via scanning electron microscopy, X-ray photoelectron and Raman spectroscopy. Based thereupon, a thorough kinetic analysis is systematically implemented by cyclic voltammetry and electrochemical impedance spectroscopy. By implementing the theory of the transmission line model and electrochemical impedance spectroscopy with symmetric cells we are able to quantitatively determine the resistance and the capacitive components of the composite electrodes. Finally, our results show that a decrease in pore resistance is key to achieve high charge transfer kinetics in electrochemical systems and discuss its possible applications on the example of next generation Na-ion batteries.

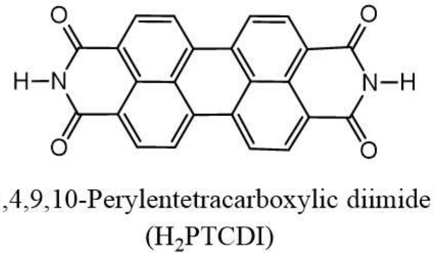

Scheme 1. Chemical structure of hydrogen terminated perylene tetracarboxylic diimide (PTCDI).

2. Results and Discussion

2.1 Morphology, Structure, and Chemical Composition

The morphology and structure of the two substrates, Cp and CuC were investigated by scanning electron microscopy (SEM).

As it is visible in the top view and cross section SEM images of the 370 μm thick Cp (Figure 1a,c), the substrate is characterized by interconnected carbon fibres with an average thickness of 7 μm. In the top view image of the CuC substrate (Figure 1b) it is shown that the substrate consists of carbon particles with a diameter ranging from 10 to 30 μm. The cross-section SEM image of CuC (Figure 1d) shows a 50 μm thick substrate, which consists of a 10 μm Cu foil and a 40 μm thick carbon particle layer on top. The carbon film consists of the described carbon particles, which are interconnected and form pores throughout the material.

The chemical composition, which was elucidated using XPS, shows also substantial differences between both carbon substrates. The surface of the samples was precleaned using 10 s Ar-ion bombardment to remove possible carbon impurities resulting from the air contact. Whereas only signals related to carbon are visible in the survey spectra of the Cp substrate, further signals resulting from sodium and oxygen are present in those obtained with the particle coated copper foil. This could be explained by the synthesis process of the carbon particle substrate, where styrene-butadiene copolymer (rubber, SBR) as binder and carboxymethylcellulose sodium (CMC, $C_8H_{16}NaO_8$) has been used. For further differentiation between the chemical states, high resolution spectra of the C 1s region were recorded. As expected, the most intense signal results from graphitic carbon (C=C) at 284.4 eV binding energy for both substrates. However, whereas for the Cp it is the only component. The surface of the carbon particles

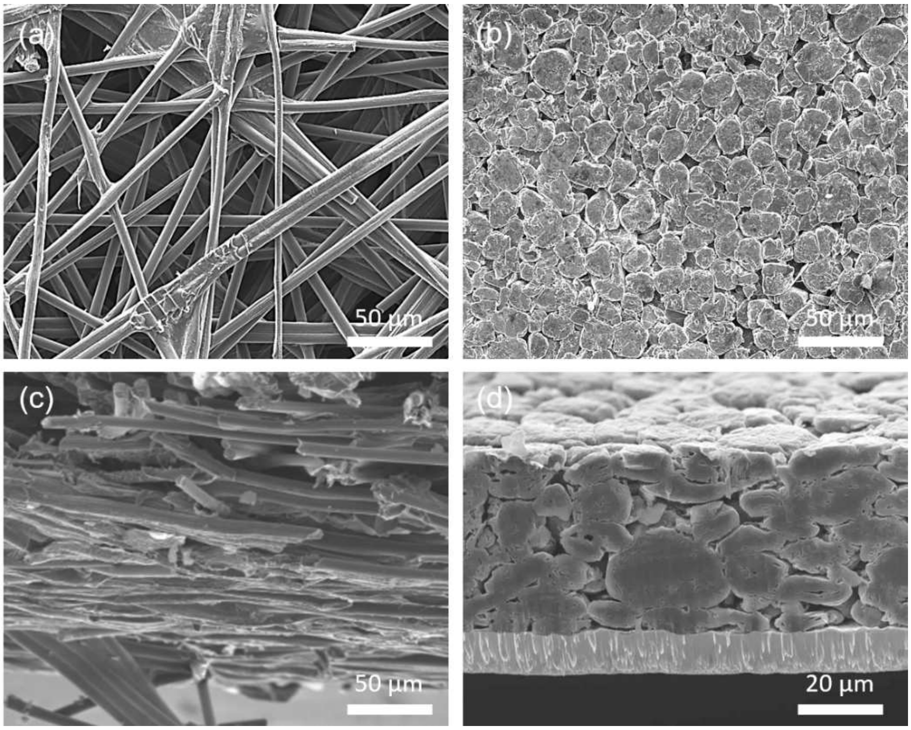

Figure 1. SEM top view (a,b) and cross section (c,d) images of (a,c) carbon paper carrier substrates and (b,d) graphite particle coated copper foil.

remains oxidized, since high amounts of oxygen-bound carbon at binding energies above 286 eV are visible in the C 1s spectrum. This difference in the chemical nature of the carbon present at the surface of the substrates also reflects in the different electrochemical behavior, which will be further discussed in the next section.

A powerful tool for the material characterization, especially for carbon-based materials as graphite, graphene and amorphous carbon species, is Raman spectroscopy, which can provide a wide range of information about the material to be examined.

Figure 3 shows the Raman spectra of Cp (grey line) and the CuC (orange line), respectively. Both spectra are characterized by the typical D, G and 2D bands for graphitic materials. The most prominent band in the spectra, the G band ($1581\ \mathrm{cm^{-1}}$) is attributed to the in-plane bond-stretching of C sp^2 pairs and is present in all Raman spectra of carbon based materials.[60–62] The FWHMs of the G band of Cp and CuC are almost identical with 23 and $22\ \mathrm{cm^{-1}}$, indicating that they are similar graphitic materials.[63] The D band ($1350\ \mathrm{cm^{-1}}$) is attributed to a ring breathing mode and is not allowed in a perfect graphitic lattice, similar to the band D′ ($1620\ \mathrm{cm^{-1}}$, a shoulder of the G band). The presence of the bands D and D′ is therefore related to the disorder and defects in the material, where the intensity ratio I_D/I_G is increasing with increasing disorder.[60–62,64–66] In addition, it is possible to calculate the cluster diameter or crystallite size L_a from the intensity ratio I_D/I_G and the laser wavelength (λ_{laser} in nm) using equation 1:[65,66]

$$L_a(nm) = \left(2.4 \times 10^{-10}\right)\lambda_{Laser}^4\left(\frac{I_D}{I_G}\right)^{-1} \tag{1}$$

The Cp substrate shows a relatively large cluster diameter with 210 nm compared to 60 nm for the CuC substrate. Further, the CuC substrate ($I_D/I_G = 0.31$) exhibits three to four times more defects than the Cp substrate ($I_D/I_G \approx 0.09$). This is also supported by the slightly more intense D+G band (~$2940\ \mathrm{cm^{-1}}$) for the CuC substrate, which is also induced by disorder. The Cp substrate is therefore a more crystalline graphitic material than the CuC substrate, which shows a more amorphous character. These findings are corroborated by XPS (Figure 2), where, for the Cp substrate, only graphitic carbon has been found, whereas for the CuC substrate also other carbonaceous species are present, which can explain the presence of disorder and defect signals in the Raman spectra of CuC. In addition to the G band, all graphitic materials exhibit a strong 2D band at ~$2700\ \mathrm{cm^{-1}}$, which corresponds to the overtone of the D band and is not symmetry depended as the D band itself is. This band shows a splitting ($2D_1$ and $2D_2$) in a three-dimensional graphite (ABABA… stacking) material, while only one band is present for single layer graphene or two-dimensional turbostratic graphite.[66,67] Since the Cp and CuC substrates show a doublet structure for the 2D signal, both materials exhibit an ordered carbon layer stacking. The

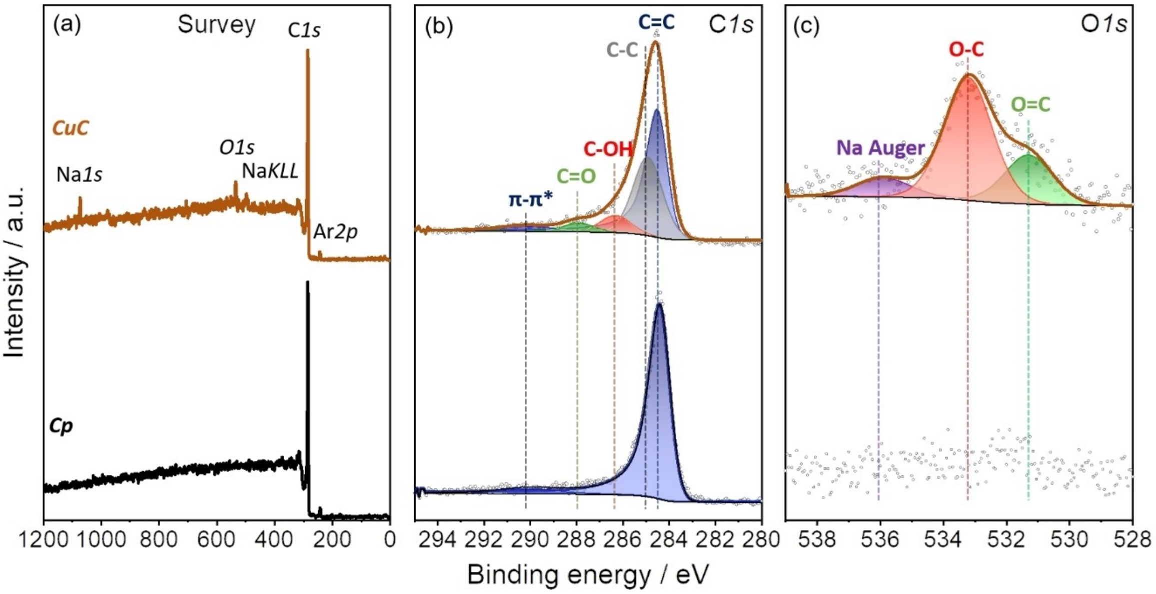

Figure 2. Elemental composition by XPS photoelectron analysis of the CuC (top) and Cp (bottom) carrier substrates. (a) Survey spectra, (b) and (c) high resolution XPS spectra of C 1s and O 1s signals, respectively.

band 2D′ at 3251 cm^{-1} is attributed to an overtone of the D′ band.[64] From the 2D band and the ratio of I_{2D}/I_G it is possible to predict electroactive properties. The Fermi levels of the investigated materials are indirect proportional to the 2D intensity and direct proportional to the 2D FWHM.[68] A low I_{2D}/I_G ratio in combination with a high FWHM of the 2D band relates to a lower energy barrier for the charge transfer and indicates a high amount of charge carriers. Both materials exhibit an equal 2D FWHM (Cp 71 cm^{-1}, CuC 70 cm^{-1}), however, the ratio I_{2D}/I_G of Cp is with 0.8 twice as high as the ratio of CuC with 0.4. CuC exhibits therefore more charge carriers than Cp and CuC is expected to show a higher electroactivity.

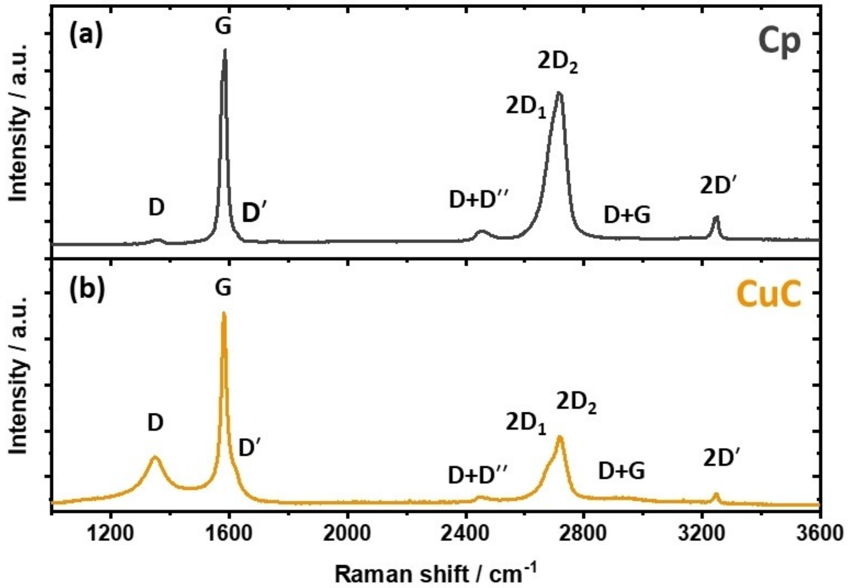

Figure 3. Raman spectra of (a) Cp, grey line and (b) CuC, orange line, from 1100 cm^{-1} to 3600 cm^{-1}, using an excitation wavelength of 532 nm.

2.2 Electrochemical Characterization

Figure 4 shows cyclic voltammetry (CV) measurements of (a) Cp and (b) CuC carrier substrates as well as PTCDI coated (c) Cp and (d) CuC at different scan rates from 200 to 0.05 mV s^{-1}. The voltammograms of pure Cp (Figure 4a) are characterized by a gradually increasing current response upon lowering the potential, typically related to a surface confined, nonfaradaic contribution arising from the charging of the electrode's double layer.[69] This behavior is found to be similar in form and shape for both substrates of Cp and CuC (Figure 4b), while the absolute specific current is significantly larger for the CuC system with a current density around -0.57 mA cm^{-2} compared to -0.20 mA cm^{-2} for Cp at 200 mV s^{-1}. A small current signal around 1.6 V for the Cp electrode and around 1.3 V for the CuC electrode has already been previously reported and is attributed to some side reaction of the substrate with the electrolyte (1 M NaFSI in EC/DMC, see Experimental Section).[37]

As previously reported,[39] the PTCDI coated Cp electrodes (Figure 4c) are characterized by two broad reduction peaks at 1.99 V, with a current density of 2.82 mA cm^{-2}, and 1.86 V, with a current density of 2.97 mA cm^{-2} (at 200 mV s^{-1}), corresponding to two one electron reductions of the PTCDI molecule, and one intense back-oxidation peak at 2.20 V, having a current density of 6.97 mA cm^{-2} (at 200 mV s^{-1}).

It is interesting to note that the redox reactions of the PTCDI molecules in the PTCDI–Cp electrode are surprisingly well resolved, even at high scan rates of 200 mV s^{-1}. The reason for this behavior has been studied in detail in our previous work, where we were able to show that the charge transfer is governed by a diffusion-less mechanism, where the transport of the Na counter ion is apparently not a limiting factor.[39] Consequently, exceptionally high charge transfer rates are possible. Since the PTCDI film is best described by a multilayer surface confined electrode, the kinetic limitation of the electrode is expected to be governed by the electron exchange reaction throughout the stacked PTCDI layers. The CV characteristics of PTCDI coated CuC electrodes (Figure 4d) are distinctively different compared to the PTCDI coated Cp electrodes. For fast scan rates of 200 mV s^{-1} the two one electron reductions of the PTCDI molecule are no longer separated but merge to one, broad reduction signal at around 1.5 V, with a current density of 3.85 mA cm^{-2}, characterized by a large polarization overpotential. A further, qualitative evolution of the CV curves with decreasing scan rate shows, that the reduction peak splits into two separate peak maxima with decreasing scan rates (Figure 4d and Figure 5a,b).

The differences in the CV measurements for the two different PTCDI coated substrates indicate a kinetic limitation with respect to the charge transfer process for the PTCDI coated CuC electrodes, which is not the case for the PTCDI coated Cp electrodes. Since the PTCDI layers and their

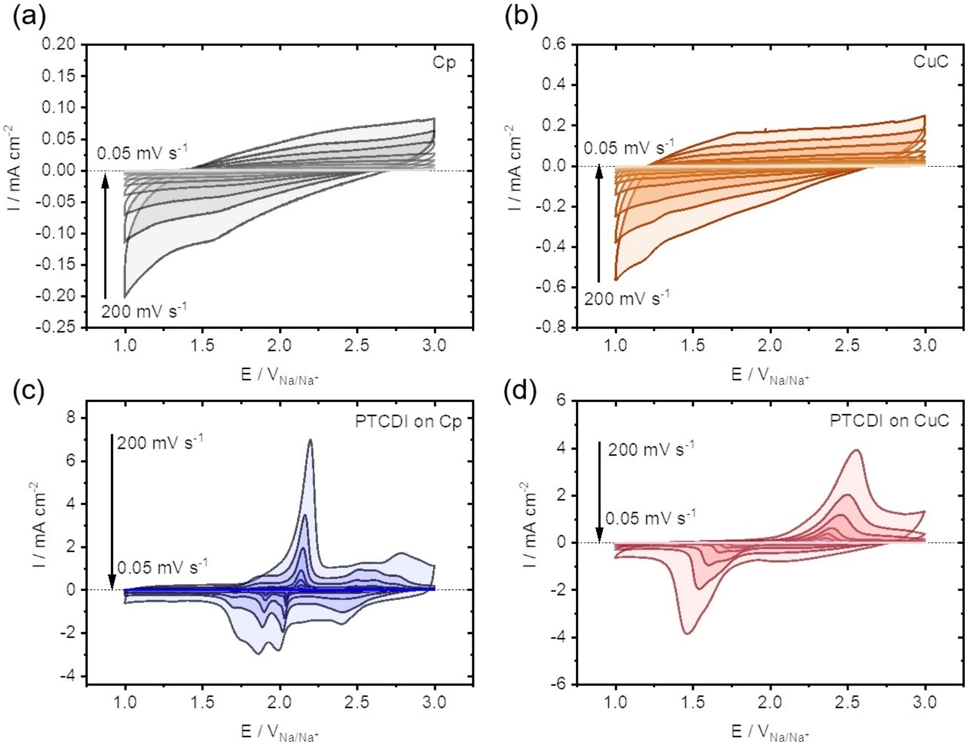

Figure 4. CV measurements of (a) Cp and (b) CuC carrier substrates and PTCDI coated (c) Cp and (d) CuC at different scan rates from 200 to 0.05 mV s^{-1} in a 1 M NaFSI in EC/DMC (1:1(v/v) mixture) electrolyte between 3.0 and 1.0 V vs. Na/Na^+.

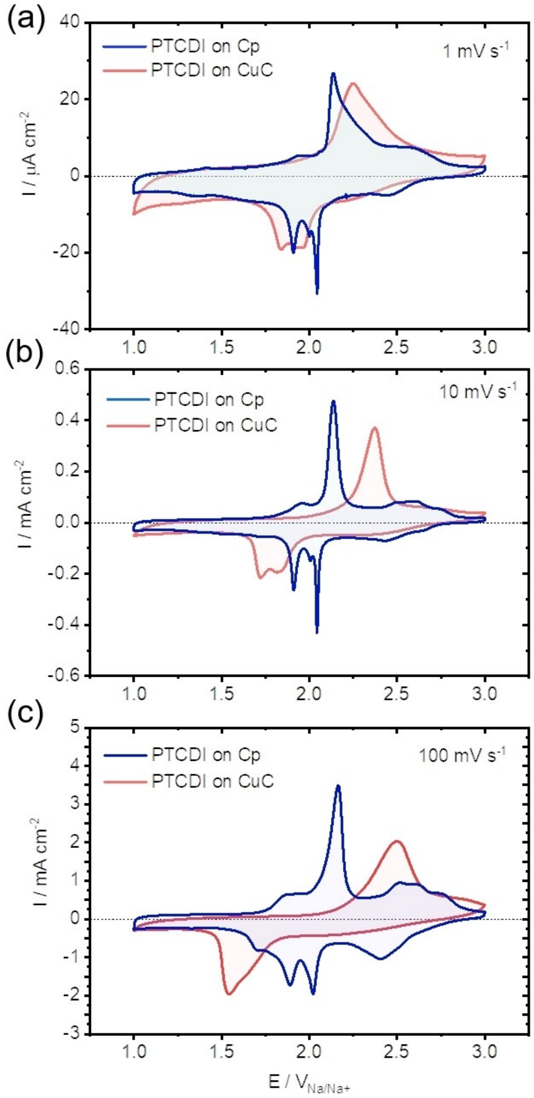

Figure 5. Direct comparison between CV measurements of PTCDI coated Cp (blue) and CuC (red) at different scan rates of (a) $1\ \mathrm{mV\,s^{-1}}$, (b) $10\ \mathrm{mV\,s^{-1}}$ and (c) $100\ \mathrm{mV\,s^{-1}}$ between 3.0 and 1.0 V vs. Na/Na^+.

deposition method are identical for both carrier substrates it can be inferred that the carrier substrate is causing the differences in the CV response. These findings are very surprising, since Raman analysis revealed that CuC exhibits more charge carriers than Cp, consequently CuC should therefore show a higher electroactivity. The CV measurements thus indicate differences at the carbon carrier to PTCDI interface in combination with Na-ion accessibility. Consequently, further kinetic analysis is performed to study the kinetic parameters and identify the prevailing charge-transfer mechanisms.

2.3 Kinetic Analysis

Electrochemical methods, such as CV and electrochemical impedance spectroscopy (EIS), have been widely used in literature to investigate the kinetic parameters and identify the charge-transfer and charge-storage mechanisms of various organic and inorganic materials.[70–72] The kinetics of the charge transfer and storage processes offer insights into the mechanisms involved as well as information about the operation of the electrochemical system.[73]

For further investigation of the substrate dependent electrochemical characteristics of Cp and CuC, the two systems are directly compared by CV measurements at several different scan rates. Figure 5 shows the comparison of CV measurements of PTCDI coated Cp (blue) and PTCDI coated CuC (red) at different scan rates of $1\ \mathrm{mV\,s^{-1}}$ (Figure 5a), $10\ \mathrm{mV\,s^{-1}}$ (Figure 5b) and $100\ \mathrm{mV\,s^{-1}}$ (Figure 5c), between 3.0 and 1.0 V.

The CV response of the two systems begin to differ significantly starting at scan rates of $1\ \mathrm{mV\,s^{-1}}$ (Figure 5a), with the difference becoming more pronounced the faster the scan rates are. For the Cp substrate system, the two most prominent reduction peak maxima at $1\ \mathrm{mV\,s^{-1}}$ are found at 2.04 V and 1.91 V, with peak current maxima of $-30.7\ \mu\mathrm{A\,cm^{-2}}$ and $-20.0\ \mu\mathrm{A\,cm^{-2}}$, respectively. Following the first reduction a small post-peak appears at about 1.99 V. The dominant back oxidation peak is observed at 2.14 V, with a peak current maximum of $26.8\ \mu\mathrm{A\,cm^{-2}}$, and is characterized by a significant tailing at slow scan rates. This tailing at small scan rates has been previously explained by kinetic limitations of the electron exchange reaction throughout the film.[39] Laviron et al. revealed in a theoretical study that for a multilayer surface confined electrode, the kinetic limitation of the charge transfer throughout the organic layers is at the beginning visible for slow scan rates, whereas the kinetic limitation of the electrochemical reaction of the first layer with the carrier substrate, here Cp, follows for faster scan rates.[74] Physically this can be interpreted as the PCTDI molecules in different layers need a slightly different energy (potential) to be reduced /oxidized, hence the broadening of the peaks.[39,74] This phenomenon seems to be more significant with decreasing scan rate. The two reduction peaks as well as the back-oxidation peak become very sharp, with peak widths (full width at half maximum) of only 42 mV, 4 mV and 56 mV at slow scan rates of $10\ \mathrm{mV\,s^{-1}}$ and less (Figure 5a,b). Upon increasing the scan rate, it is found that the peak potentials of PTCDI coated Cp remain almost constant up to $50\ \mathrm{mV\,s^{-1}}$. At a scan rate of $100\ \mathrm{mV\,s^{-1}}$ (Figure 5c) a small but noticeable deviation from the constant potential is observable, as the reduction peak potentials shift to more cathodic potentials (2.02 V and 1.89 V) and the oxidation peak potential shifts to a more anodic potential (2.16 V). The constant peak potentials over this wide range of scan rates indicate the reversibility of the redox reaction under these conditions, but unlike the ideal behavior of a reversible surface confined systems, the peak potentials of the reduction and oxidation reactions are not at the same potential, even for slow scan rates.[75] The difference between the peak potentials is around 90 mV. The reason for this non-ideal behavior has been attributed to an attractive intermolecular interaction between the PTCDI molecules.[39,74–76]

The CV response for the CuC substrate system is clearly different to the Cp substrate for scan rates at, and above 1 mV s^{-1} (Figure 5a). The redox peaks for PTCDI on CuC are much broader, even at small scan rates, with a significant polarization overpotential. Furthermore, the reduction and oxidation peaks shift strongly to more cathodic and anodic potentials upon increasing the scan rate. While at 1 mV s^{-1} the 1st and 2nd reduction peaks are at 1.97 V and 1.84 V, respectively, their potentials shift by −140 mV and −120 mV to 1.82 V and 1.72 V, when the scan rate is increased to 10 mV s^{-1} (Figure 5b). At 100 mV s^{-1} (Figure 5c) the two reduction peaks merge to one broad reductive wave with a peak maximum around 1.54 V and a peak current of 1.96 mA cm^{-2}.

The amount of charge transferred at high scan rates of 100 mV s^{-1} (Figure 5c), obtained by integrating the current-time signal in the CV response, appears to be quite similar between the two systems, with 615 C g^{-1} for PTCDI on Cp and 610 C g^{-1} for PTCDI on CuC. However, the kinetics seem to be remarkably different. The minimal shift in the peak potentials upon increasing the scan rate from 1 mV s^{-1} to 100 mV s^{-1} for PTCDI on Cp indicate that the charge-transfer is mostly independent of the sweep rate. Redox peaks that exhibit small voltage offsets even at high rates are indicative for pseudocapacitive materials.[69,77–79]

In general, electrochemical charge transfer processes can be divided into diffusion- controlled and surface- controlled processes. Surface- controlled processes can be further subdivided into the faradaic contribution from the charge-transfer process with surface atoms, referred to as pseudocapacitance, and the nonfaradaic contribution arising from the charging of the double layer.[69]

The capacitive effects are characterized by analyzing the CV data at various sweep rates, following a method developed by Hagfeldt, Lindquist and co-workers,[80] in which the capacitive contributions can be quantitatively separated from the total charge. The current response, as a function of the sweep rate, is found to follow a relatively simple power law dependence, applied before for the investigation of Li$^+$ insertion into nanoporous anatase films and nanoparticles,[80,81] according to equation 2:

$$\mathrm{I} = \mathrm{a}\nu^{\mathrm{b}} \tag{2}$$

where the measured current (I) follows a power law relationship with the sweep rate ν. Both *a* and *b* are adjustable parameters. There are two well-defined conditions: $b = 0.5$ and $b = 1.0$. For $b = 0.5$, the current is proportional to the square root of the scan rate, which points to a diffusion controlled, faradaic process, according to the following equation 3:

$$I = nFACD^{1/2}\nu^{1/2}\left(\frac{\alpha nF}{RT}\right)^{1/2}\pi^{1/2}\chi^{(bt)} \tag{3}$$

where *C* is the surface concentration of the electrode material, α, is the transfer coefficient, *D* is the chemical diffusion coefficient, *n* is the number of electrons involved in the electrode reaction, *A* is the surface area of the electrode materials, *F* is the Faraday constant, *R* is the molar gas constant, *T* is the temperature, and the $\chi(bt)$ function represents the normalized current for a totally irreversible system as indicated by the CV response.

The other defined condition, $b = 1.0$, represents a capacitive response, where the capacitive current is proportional to the sweep rate, according to equation 4:

$$\mathrm{I} = \nu \mathrm{C_d A} \tag{4}$$

where C_d is the capacitance and *A* is the surface area of the active electrode material. Accordingly, the current response at any given potential can then be expressed as being the combination of two separate mechanisms, the surface capacitive effects and the diffusion controlled, faradaic processes, according to equation 5:

$$I(V) = k_1\nu + k_2\nu^{1/2} \tag{5}$$

In equation 5, $k_1\ \nu$ and $k_2\ \nu^{1/2}$ correspond to the current contributions from the surface capacitive effects and the diffusion controlled, faradaic processes, respectively. Thus, by determining k_1 and k_2 it is possible to quantify, at certain potentials, the fraction of the current due to each of these contributions. By plotting the current as a function of potential divided by $\nu^{1/2}$ over $\nu^{1/2}$, the slope of the linear fit will allow to determine k_1, while the intercept with the y-axis will allow to determine k_2. These concepts introduced above are used to describe, according to equation 5, the current response at any given potential as the combination of surface capacitive and diffusion controlled processes.[80,81] As shown in Figure 6a, the diffusion controlled current at 0.1 mV s^{-1} for PTCDI coated Cp is mainly created at or around the peak potentials of the PTCDI reduction. The capacitive current contribution for PTCDI coated Cp (Figure 6a, grey shaded area) is somehow following the overall CV response with maxima at the beginning of the reduction wave and at the end of the oxidation wave. This shows that the capacitive current contribution is, to a large extent related to the charge-transfer process with the PTCDI molecules and can therefore be classified as pseudocapacitive.

While at a sweep rate of 0.1 mV s^{-1} it is found that both, the diffusion- controlled and the pseudocapacitive- controlled charge transfer processes are equally present for the PTCDI coated Cp (57 % : 43 %), further analysis at different scan rates reveal, that the pseudocapacitive contribution steadily increases with increasing scan rate. At, for example, a scan rate of 10 mV s^{-1} (Figure 6b), the pseudocapacitive contribution is

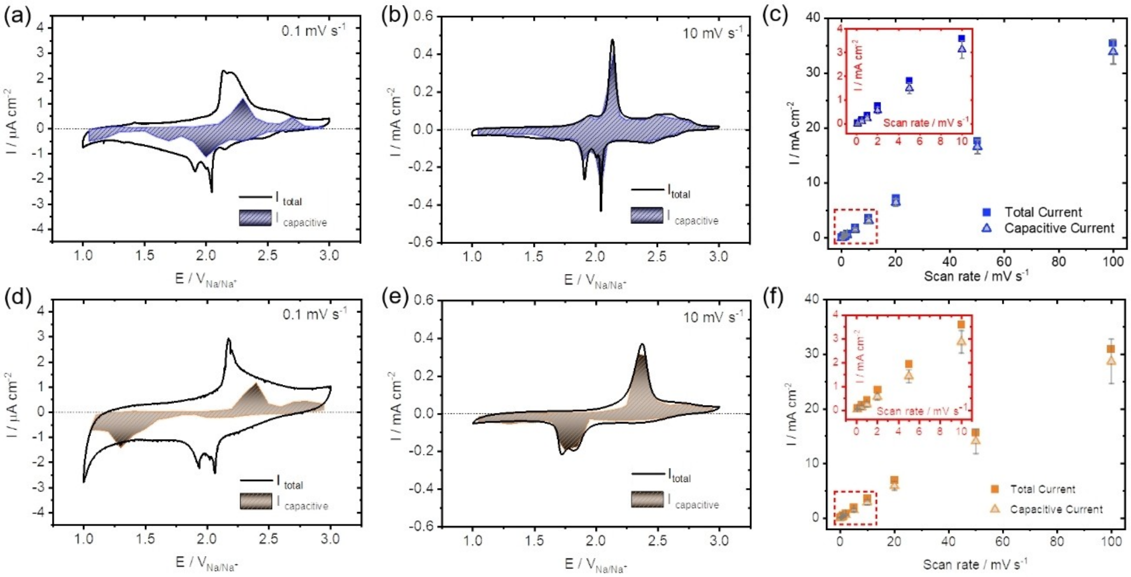

Figure 6. Separation of capacitive (gray shaded area) and total (black line) currents in CV measurements of PTCDI coated (a,b) Cp and PTCDI coated (d,e) CuC at two different scan rates of (a,d) 0.1 and (b,e) 10 mV s^{-1}, respectively. A detailed separation of the capacitive and total currents at various scan rates between 0.1 and 100 mV s^{-1} is shown in (c) for PTCDI coated Cp and (f) for PTCDI coated CuC (inset: detailed view of the slow scan rates highlighted by the red dashed area).

clearly dominant with a contribution of 87% to the overall current response. The detailed contribution of the pseudocapacitive to the total currents at various scan rates between 0.1 and 100 mV s^{-1} for the PTCDI coated Cp is shown in Figure 6c.

When the pseudocapacitive contribution to the total current response is compared between PTCDI coated Cp and PTCDI coated CuC electrodes, significant differences are observed. At a sweep rate of 0.1 mV s^{-1} the pseudocapacitive contribution for the CuC electrodes (Figure 6d, grey shaded area) is significantly lower compared to the PTCDI coated Cp electrodes, with 25% compared to 43%, respectively. Also, the pseudocapacitive charge transfer maxima are further shifted to more negative potentials for the reductive contribution and to more positive potentials for the oxidative contribution. This difference in pseudocapacitive contribution between the two carrier substrates becomes less as the scan rate is increased. At a scan rate of 10 mV s^{-1}, also the current response of PTCDI coated CuC electrodes is mainly pseudocapacitive, with 77% (Figure 6e). The comparison of the overall contribution of pseudocapacitive to the total current for various scan rates between 0.1 and 100 mV s^{-1} shows, that for all scan rates investigated, the PTCDI coated CuC electrodes are stronger diffusion controlled compared to the PTCDI coated Cp electrodes (Figure 6c,f). This fact can be even better seen in the fully quantified contribution ratios of the capacitive and diffusion-controlled currents versus scan rate for the two different PTCDI coated carrier substrates as depicted in Figure 7b,d.

Figure 7 shows the separation of pseudocapacitive and total currents in the CV measurements of PTCDI coated Cp (Figure 7a) and PTCDI coated CuC electrodes (Figure 7c) at 1 mV s^{-1} where, in the beginning, distinctive differences in the CV responses between the two systems have been observed (Figure 5a). At this specific scan rate, the current response for the PTCDI coated Cp electrodes is already largely determined by a pseudocapacitive contribution at and around the redox peak maxima. This is not the case for the PTCDI coated CuC electrodes where initially the peak onset currents are mainly diffusion controlled. The quantitative contribution ratios of the capacitive and diffusion-controlled currents for the CV measurements shown in Figure 7a,c are highlighted in Figure 7b,d.

This is a very interesting finding, especially since previous analysis of CV measurements on PTCDI coated Cp revealed a diffusion-less mechanism, suggesting that charge balance by the Na counter ion (and consequently Na ion storage in battery applications) in a PTCDI film allows for exceptionally fast charging/discharging rates.[39] This can now be evidently understood, since for a surface redox reaction with pseudocapacitive charge transfer to the surface redox materials (here the PTCDI molecules), the charge transfer mechanism is attributed to the transfer occurring at or near the surface of the material where ions are electrochemically adsorbed. This is creating very short diffusion distances and, consequently, short diffusion times. From this analysis it is obvious that the carrier substrate morphology and structure is a crucial component for the charge transfer kinetics at electrodes related to electrochemical energy conversion and storage technologies. The micro- and nano-sized dimensions of our PTCDI coated Cp or CuC electrodes (see SEM images in Figure 1) create an electronically conductive particle network, where the pores are

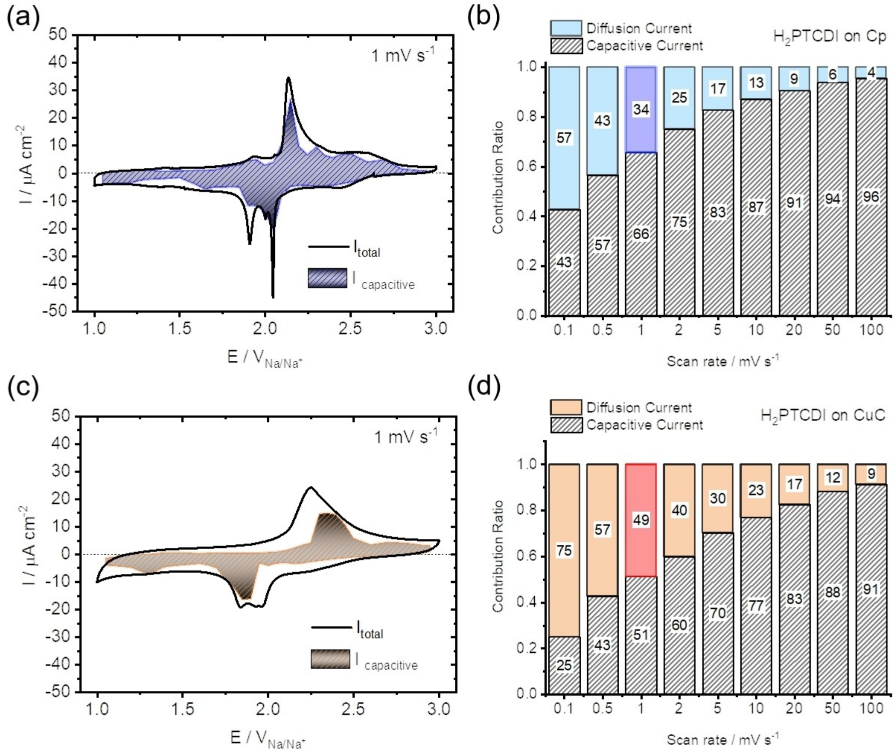

Figure 7. Separation of capacitive (gray schaded area) and total (black line) currents in CV measurements of PTCDI coated (a) Cp and PTCDI coated (c) CuC at 1 mV s^{-1}. (b,d) Contribution ratio of the capacitive and diffusion-controlled charge versus scan rate for PTCDI coated (b) Cp and PTCDI coated (d) CuC electrodes.

filled with electrolyte. For an efficient charge-transfer reaction, both, the electron transport in the conductive carrier substrate, and the ionic transport through the electrolyte filled pores have to be well balanced. Since the electric conductivity of carbon and its allotropes (i.e. graphite, hard carbon, glassy carbon) is several orders of magnitude larger ($\sigma_{cc} \approx 10^2$–10^4 S/cm) than the ionic conductivity of the electrolyte ($\sigma_{el} \approx 10^{-2}$ S/cm),[82] the kinetic limitations are expected to originate mainly form the pore resistance that is related to the ion movement in the electrolyte.

To further investigate and understand why the charge transfer for the PTCDI coated CuC electrodes is strongly kinetically influenced by ion diffusion, while this is not the case for the PTCDI coated Cp electrodes, electrochemical impedance spectroscopy is performed on these two systems.

2.4 Electrochemical Impedance Spectroscopy

Electrochemical impedance spectroscopy (EIS) is one of the most utilized electrochemical methods to characterize electrode materials relevant to energy conversion and storage technologies, including heterojunction and dye-sensitized solar cells,[83–86] rechargeable batteries,[37,87–91] and electrocatalysts/photocatalysts for water splitting and CO_2 reduction.[92–95] EIS is a non-destructive tool that allows to investigate and differentiate several interfaces like solid/electrolyte or solid/solid, within a devices on the basis of their frequency response under potential control and the subsequent decoupling of resistive and capacitive circuit components.[96] Therefore, EIS allows to study these components independently based on the frequency dependent current response of the electrode. Differently, a direct current technique such as cyclic voltammetry (CV) always shows capacitive and resistive features simultaneously.

In order to analyze and extract meaningful data from EIS measurements, the measured impedance response is fitted to an equivalent circuit model (EEC) which combines fundamental elements such as resistors, capacitors, inductors and constant phase elements.[71,97,98] The impedance response of the electrolyte filled pores in an electronically conductive particle network, such as in our PTCDI coated Cp or CuC electrodes, can be described by an equivalent circuit model referred to as transmission-line model (TLM).[99]

In order to determine the pore resistance of the PTCDI coated CuC and Cp substrates by impedance analysis, symmetrical electrochemical cells (Figure 8a) were built using the porous PTCDI coated electrodes as working and counter electrode with an electrolyte filled glassfiber separator in between. In the technique of impedance spectroscopy with symmetric cells two electrodes are used as both electrodes of a symmetric cell to perform impedance measurements, conse-

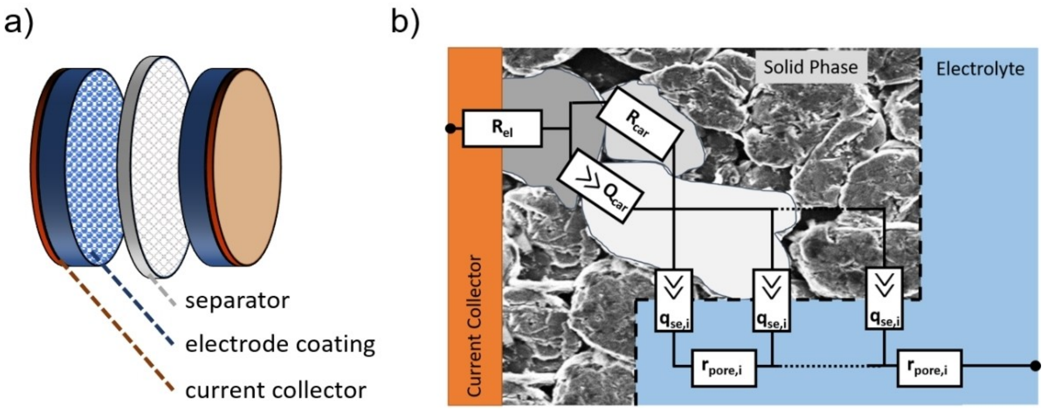

Figure 8. (a) Schematic arrangement of a symmetric battery-cell for pore resistance analysis with the electrodes facing each other. The separator between the porous electrodes and the electrodes are soaked with electrolyte. (b) Schematic representation of the EEC model employing a transmission-line model for the porous electrode. The charge transfer process between the solid and the liquid interphase is modelled via q_{se} through faradaic or capacitive charge transfer reactions electrons are moving in the solid phase (graphite particle), while ions are moving in the liquid electrolyte phase (blue region).

quently, since a single impedance spectrum is obtained, a detailed analysis of the internal resistance is possible.[99,100] The use of the glassfiber separator is not mandatory for this type of analysis but proved to be advantageous in order to prevent an electronic shortcircuit between the two electrodes and to keep the electrodes in a plane-parallel configuration at a constant distance of approx. 1 mm.

Figure 8b shows a schematic drawing of the EEC model employing a transmission-line model for fitting the impedance response of the porous electrodes. R_{el} is the sum of all ohmic resistances including resistance due to wires, contacts between the current collector and the carbon particle network and solutions, R_{car} is the electronic resistance in parallel to the corresponding capacitance (Q_{car}) originating mainly from the interfaces of the solid phase carbon carrier particles. The vertical infinitesimal impedances q_s represent the impedance response at the interface between electrolyte and the surface area of the active material (PTCDI). Since our system is assumed to be under blocking conditions, i.e. in the absence of faradaic charge transfer reactions, the surface impedance elements are modelled via a constant phase element Z_Q with the electrode's double layer capacitance Q, angular frequency ω, constant phase exponent α and the imaginary unit $\boldsymbol{j}$. The infinitesimal impedances of the L-long TLM add up to:

$$Q = L \cdot q_{se} = \sum_{i}^{n} \frac{1}{q_{se,i}} \tag{6}$$

$$Z_Q = \frac{1}{Q\ (\boldsymbol{j}\omega)^{\alpha}} \tag{7}$$

The lower chain of the of the TLM represents the infinitesimal pore resistances ($r_{pore,i}$), which sums up to R_{pore} for the L-long TLM by:

$$R_{pore} = L \cdot r_{pore,i} = \sum_{i}^{n} r_{pore,i} \tag{8}$$

The impedance of the TLM under blocking conditions is then given by:

$$Z_{TLM,block} = \sqrt{\frac{R_{pore}}{Q\ (\boldsymbol{j}\omega)^{\alpha}}} \cdot \coth\left(\sqrt{R_{pore} \cdot Q\ (\boldsymbol{j}\omega)^{\alpha}}\right) \tag{9}$$

Equation 9 has previously been used to model the electrochemical impedance of a porous cathode catalyst layer in polymer electrolyte fuel cells by Eikerling et. al.,[101] and the impedance of porous Li-ion battery electrodes and separators by Landesfeind et. al.,[99] quite effectively.

For Li-ion batteries, blocking conditions were shown to be approached at 0% state of charge.[100,102,103] In order to fulfill this prerequisite, EIS measurements were performed in this work at open circuit potential (OCP) where steady-state conditions were assured during EIS measurements since the OCP value has been maintained practically constant. We further verified the applicability of this method via realizing blocking conditions using the non-intercalating electrolyte salt $TBAPF_6$, which is stable within the potential window of the impedance measurement (±10 mV), instead of NaFSI and keeping all other parameters identical. Both electrolyte salts gave similar results.

Figure 9 shows Nyquist and Bode plots measured under blocking conditions (0% state of charge) for Cp, PTCDI coated Cp, CuC and PTCDI coated CuC and the corresponding EEC fits (dashed lines) following the transmission-line model shown in Figure 8b. In the Nyquist plot, the impedance is plotted as a complex plane plot with Z_{Im} ($-\mathrm{Im}/\Omega$) along the y-axis and Z_{Re} (Re/Ω) along the x-axis. In the Bode plots (Figure 9c,f) two plots are combined which show the

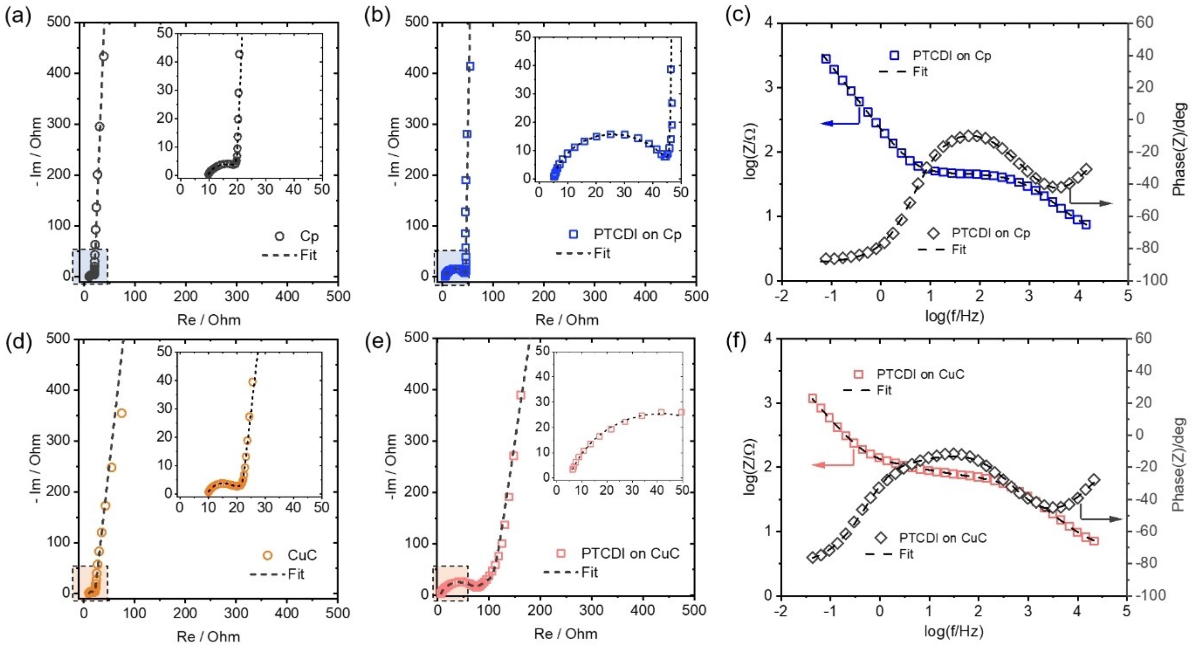

Figure 9. Nyquist plots and corresponding EEC fits of (a) Cp, (b) PTCDI coated Cp, (d) CuC and (e) PTCDI coated CuC (inset: detailed view of the high frequency area highlighted by the colour shaded square). Bode plots of the impedance data for (c) PTCDI coated Cp and (f) PTCDI coated CuC electrodes, respectively.

logarithm of the magnitude of impedance $|Z|$ and the phase angle ϕ on the y-axis over the logarithm of the modulation frequency f (in Hz) along the x-axis, giving the frequency dependence of the impedance.

All Nyquist plots (Figure 9a,b,d,e) are characterized by a small offset at the real axis representing the initial series resistance R_{el}, followed by a slightly depressed semicircle arc at high frequencies of 200 kHz. This characteristic semicircle arc can be ascribed to the parallel combination of R_{car}, the electronic charge transfer resistance and the corresponding capacitance (Q_{car}, modelled with a constant phase element), originating mainly from the interfaces of the solid phase particles as depicted in Figure 8b. At frequencies lower than 100 to 200 Hz, the semicircle arc progresses into an almost straight and vertical low frequency branch that is characteristic for a transmission-line model that allows to determine the ionic resistance in the porous electrodes (R_{pore}) according to equation 9.[99,103] In the case of the PTCDI coated electrodes (Figure 9b,e) the plots reveal an additional linear part with an almost 45° slope at medium frequencies between 30 and 2 Hz. This 45° slope in the medium frequency region reflects a Warburg like ionic diffusion resistance in the PTCDI coated porous electrodes and is found to be most dominant for the PTCDI coated CuC electrodes.[100]

Further analysis of the impedance data to obtain quantitative information has been achieved by fitting the measured data to the EEC model depicted in Figure 8b. As can be seen in the Nyquist plots (Figure 9a,b,d,e) and even better in the Bode plots (Figure 9c,f), the fitting curve (dashed line) represents the measured data quite well. One has to point out that the Nyquist plots in this work do not show a perfectly vertical low frequency branch, accordingly the accuracy of the EEC transmission-line model fit will largely depend on the selected low-frequency cutoff in the fitting procedure.[99,102] For this analysis the corresponding best fits where obtained to an accuracy where the mean square deviation (X^2/Z), weighed by the impedance modulus, is below 1%, in the frequency range from 100 kHz to 30 mHz. Table 1 gives a detailed summary over all fitting parameters obtained for the four systems shown in the Nyquist plots of Figure 9.

From Table 1 it can be seen that R_{el} is quite small (4.5–9.6 Ω) for all four systems. Interestingly, it is found that for both, PTCDI on Cp and PTCDI on CuC, the R_{el} is significantly smaller compared to the uncoated substrates. This is at first counter intuitive and the reason for this observation should be further investigated in the future. The charge transfer resistance at the interface R_{car} is significantly increased when a

Table 1. Summary of all fitting parameters for the Nyquist and Bode plots shown in Figure 9. Parameters have been fitted by a Randomize + Simplex algorithm with a weighed Z using the EC-Lab Software V11.01.

	Cp	PTCDI on Cp	CuC	PTCDI on CuC
R_{el}/Ohm	9.5	4.9	9.6	4.5
C_{car}/μF	3.7	4.5	1.1	4.8
R_{car}/Ohm	7.5	38.3	8.9	59.8
R_{pore}/Ohm	8.5	9.2	9.7	128.0
τ/ms	0.8	6.4	2.0	300
α	0.98	0.99	0.93	0.91

PTCDI film is present with 38.3 Ω for the PTCDI on Cp and 59.8 Ω for the PTCDI on CuC electrodes. This is expected, since the PTCDI film is considerably less conductive than the carbon particles. Intriguingly though, while the ionic resistance in the pores (R_{pore}) is, with 9.2 Ω, significantly lower than the charge transfer resistance (38.3 Ω) for PTCDI coated Cp electrodes, the opposite is observed for the PTCDI coated CuC electrodes, with 128 Ω to 59.8 Ω, respectively (Table 1). As a result, the kinetics of the PTCDI coated CuC electrodes are strongly reduced, since the total electrode resistance is now heavily influenced by both R_{pore} and R_{car}. Consequently, the characteristic diffusion time (τ) is also substantially increased from 2.0 ms to 300 ms for PTCDI coated Cp and PTCDI coated CuC electrodes, respectively. The rate-determining process for the PTCDI coated CuC electrodes is therefore, different to the PTCDI coated Cp electrodes, the conduction of the Na counter ions through the porous channels of the electrode. Accordingly, the reaction in the depth direction is delayed, which is totally corroborated by the difference in the CV measurements at elevated scan rates, shown in Figure 5.

We have to point out that the total electrode resistance of the PTCDI coated CuC electrodes is greatly affected by the porous structure, especially for thick electrodes at a high loading with the active material. In the case of PTCDI coated Cp electrodes the charge transfer reaction is fast since only R_{car} ads significantly to the electrode resistance. It is therefore important to note that experimentally observed rate capabilities for thin film organic electrodes (such as 200 nm PTCDI coatings) make only small contributions to the actual charge transfer kinetics of an electrochemical cell, if porous substrates with a high ionic resistance in the pores are used.

3. Summary and Outlook

In Summary, this work investigates the role of two different conductive carbon substrates, CuC and Cp, coated with a thin film of perylentetracarboxylicdiimide (PTCDI) as the active electrode material. SEM images reveal the micro- and nano-sized dimensions of the PTCDI coated Cp or CuC electrodes that create an electronically conductive particle network, where the pores are filled with electrolyte. XPS and Raman spectroscopy reveal substantial differences between both systems regarding their morphology, structure, and chemical composition. Raman spectroscopy showed that both substrates are graphitic materials, but they differ substantially from each other. The carbon fibers of Cp are composed of 210 nm clusters and the material shows almost no defects in the graphitic lattice. In contrast, CuC exhibits more defects in the graphitic lattice and a higher charge transfer carrier density with smaller domains of about 60 nm and thus a more amorphous structure than Cp. This is also supported by XPS analysis, which essentially detects only sp^2 C in Cp. In contrast, a substantial amount of sp^3 C and further oxidized carbonaceous species is also visible in the spectra of CuC, which is characteristic of the defects in the graphitic material.

Consequently, the electrochemical CV response of the two systems is observed to differ significantly with respect to peak potentials and peak current densities, starting at scan rates of 1 $mV\,s^{-1}$, with the difference becoming more pronounced the faster the scan rates are. A thorough kinetic analysis using CV measurements at different scan rates reveals significant pseudocapacitive current contributions at and around the redox peak maxima, even at slow scan rates for the PTCDI coated Cp electrodes. Differently, for the PTCDI coated CuC electrodes, initially the peak onset currents are mainly diffusion controlled and consequently kinetically limited. Further investigation of the charge transfer kinetics by using electrochemical impedance spectroscopy with symmetric cells and implementing the theory of the transmission line model allowed for a quantitative analysis of the resistance and capacitive components of the composite electrodes. It is found that the total internal electrode resistance of the PTCDI coated CuC electrodes is greatly affected by the ionic resistance in the pores, which can be attributed to the substrate's porous structure. Differently, in the case of PTCDI coated Cp electrodes, the charge transfer reaction is fast since its pore resistance has only a negligible contribution towards the overall internal resistance.

This work shows that a low pore resistance is very important to achieve high charge transfer kinetics in electrochemical systems using porous carbon carrier substrates, like in Na-ion batteries. These insights into the substrate dependent charge transfer kinetics will therefore contribute towards future, efficient electrode design and may proof of great importance for the development of various energy conversion and storage technologies.

4. Experimental Section

Material synthesis: Carbon paper (Cp, MGL370, AvCarb, thickness: 0.3 mm) and graphite/copper (CuC, MTI Corporation, single layer CMS graphite coated, thickness: 0.05 mm) discs with a diameter of 17 mm were punched out. Commercially available 3,4,9,10-Perylene-Tetracarboxylic Diimide (H_2PTCDI, TCI Chemicals, > 95 %) was purified by vacuum sublimation in a tube furnace at 380 °C for 5 h prior to evaporation. Evaporation of 250 nm thin films of the PTCDI compounds was done under vacuum ($\sim 1\text{–}2{*}10^{-6}$ mbar) using a custom-built organic evaporation system from Vaksis R&D and Engineering, allowing precise rate control (1.2 $Å\,s^{-1}$) and material heating (at 340 °C).

Scanning electron micrographs (SEM): A CrossBeam NVision 40, Zeiss instrument was used and images were acquired with an electron acceleration voltage of 5 kV using the secondary electron detector.

X-ray photoelectron spectroscopy (XPS): A Multi-Lab2000 instrument (ThermoFisher Scientific, U.K.) equipped with a monochromatic X-ray source (Al Kα, 1486.6 eV) and a hemispherical analyzer (ThermoFisher Scientific) was utilized for spectra acquisition. Charge compensation was carried out by the emission of electrons at a kinetic energy of 6 eV via a flood gun. All spectra were shifted with respect to the graphitic/*sp*^{2} carbon (C=C) component at 284.4 eV. High resolution spectra were recorded with a pass energy of 20 eV. Before each measurement, the samples were cleaned by Ar sputtering (3 keV, ion current of 1.0 µA) for 20 s. Peak deconvolution was performed with the software CasaXPS.[104]

Raman: The Raman measurements were detected by a WITec alpha300R confocal Raman microscope and using a green laser (532 nm, 20 mW) through a Zeiss Neofluar objective (40x magnification). The spectra were collected through a 600 g/mm-grating with the spectral centre set at 1900 rel. cm^{-1} and recorded with a CCD-camera (integration time: 5 minutes). The software WITec Suite FIVE was employed for cosmic ray removal and background subtraction.

Electrochemical cell assembling and electrochemical measurements: The electrochemical measurements were carried out in a three electrode ECC-Ref Cell (El-Cell) using a Biologic VMP3 potentiostat at room temperature. Sodium metal (Na rod in paraffin oil, VWR, 99.5 %) was used as counter and reference electrode and a glass fiber disc (Ø = 18 mm, thickness 1.55 mm, El-Cell) as separator. The electrolyte (Solvonic, 99 %) used was 1 M NaFSI (sodium bis (fluorosulfonyl)imide) in a 1 : 1 (v/v) mixture of ethylene carbonate (EC) and dimethylcarbonate (DMC). The cells were produced in an Ar-filled glove box (UNI-lab, MBraun) with a water and oxygen content below 0.1 ppm. EIS were carried out in a frequency range from 100 kHz to 10 mHz with a symmetrical two-electrode cell setup using the same glass fiber disc separator and electrolyte as described above.

Acknowledgements

We gratefully acknowledge the support of the Austrian Science Foundation (FWF) within the FWF project P29645-N36. Furthermore, we gratefully acknowledge the continuous support of Prof. Niyazi Serdar Sariciftci at the Linz Institute for Organic Solar Cells (LIOS) at the Johannes Kepler University of Linz.

References

[1] R. Kerr, *Science (80-.).* **2007**, *317*, 437.

[2] J. Tollefson, *Nature* **2019**, *574*, 17–18, DOI:10.1038/d41586-019-02897-7.

[3] O. Hoegh-Guldberg, D. Jacob, M. Taylor, T. Guillén Bolaños, M. Bindi, S. Brown, I. A. Camilloni, A. Diedhiou, R. Djalante, K. Ebi, et al., *Science* **2019**, *365*, eaaw6974, DOI:10.1126/science.aaw6974.

[4] M. I. Hoffert, K. Caldeira, A. K. Jain, E. F. Haites, L. D. D. Harvey, S. D. Potter, M. E. Schlesinger, S. H. Schneider, R. G. Watts, T. M. L. Wigley, et al., *Nature* **1998**, *395*, 881–884, DOI:10.1038/27638.

[5] M. Mikkelsen, M. Jørgensen, F. C. Krebs, *Energy Environ. Sci.* **2010**, *3*, 43, DOI:10.1039/b912904a.

[6] J. Turner, *Science* **1999**, *285*, 687–9.

[7] T. R. Cook, D. K. Dogutan, S. Y. Reece, Y. Surendranath, T. S. Teets, D. G. Nocera, *Chem. Rev.* **2010**, *110*, 6474–502, DOI:10.1021/cr100246c.

[8] G. a Olah, G. K. S. Prakash, A. Goeppert, *J. Am. Chem. Soc.* **2011**, *133*, 12881–98, DOI:10.1021/ja202642y.

[9] V. Sgobba, D. M. Guldi, *Chem. Soc. Rev.* **2009**, *38*, 165–84, DOI:10.1039/b802652c.

[10] J. Lach, K. Wróbel, J. Wróbel, A. Czerwiński, *Energies* **2021**, *14*, 2649, DOI:10.3390/en14092649.

[11] F. Bonaccorso, L. Colombo, G. Yu, M. Stoller, V. Tozzini, A. C. Ferrari, R. S. Ruoff, V. Pellegrini, *Science* **2015**, *347*, 1246501, DOI:10.1126/science.1246501.

[12] A. C. Ferrari, J. Robertson, *Philos. Trans. R. Soc. London Ser. A* **2004**, *362*, 2477–2512, DOI:10.1098/rsta.2004.1452.

[13] J. Robertson, *Mater. Sci. Eng. R* **2002**, *37*, 129–281, DOI:10.1016/S0927-796X(02)00005-0.

[14] E. H. Falcao, F. Wudl, *J. Chem. Technol. Biotechnol.* **2007**, *82*, 524–531, DOI:10.1002/jctb.1693.

[15] K. Gong, Y. Yan, M. Zhang, L. Su, S. Xiong, L. Mao, *Anal. Sci.* **2005**, *21*, 1383–1393, DOI:10.2116/analsci.21.1383.

[16] S. Iijima, *Nature* **1991**, *354*, 56–58, DOI:10.1038/354056a0.

[17] S. Iijima, T. Ichihashi, *Nature* **1993**, *363*, 603–605, DOI:10.1038/363603a0.

[18] N. S. Sariciftci, A. J. Heeger, *Synth. Met.* **1995**, *70*, 1349–1352, DOI:10.1016/0379-6779(94)02874-X.

[19] M. A. Deshmukh, S.-J. Park, B. S. Hedau, T.-J. Ha, *Sol. Energy* **2021**, *220*, 953–990, DOI:10.1016/j.solener.2021.04.001.

[20] M. Aftabuzzaman, C. Lu, H. K. Kim, *Nanoscale* **2020**, *12*, 17590–17648, DOI:10.1039/D0NR04112B.

[21] A. Bedeloglu, P. Jimenez, A. Demir, Y. Bozkurt, W. Maser, N. S. Sariciftci, *J. Text. Inst.* **2011**, *102*, 857–862, DOI:10.1080/00405000.2010.525816.

[22] L. Leonat, M. S. White, E. D. Głowacki, M. C. Scharber, T. Zillger, J. Rühling, A. Hübler, N. S. Sariciftci, *J. Phys. Chem. C* **2014**, *118*, 16813–16817, DOI:10.1021/jp5020912.

[23] N. S. Sariciftci, L. Smilowitz, A. J. Heeger, F. Wudl, *Science* **1992**, *258*, 1474–1476, DOI:10.1126/science.258.5087.1474.

[24] Y. Wang, C. Zhang, X. Li, T. Gao, X.-B. Wang, *Mater. Res. Bull.* **2021**, *140*, 111294, DOI:10.1016/j.materresbull.2021.111294.

[25] X. Huang, T. Shen, S. Sun, Y. Hou, *ACS Appl. Mater. Interfaces* **2021**, *13*, 6989–7003, DOI:10.1021/acsami.0c19922.

[26] D. Wielend, M. Vera-Hidalgo, H. Seelajaroen, N. S. Sariciftci, E. M. Pérez, D. R. Whang, *ACS Appl. Mater. Interfaces* **2020**, 12, 32615-32621, acsami.0c06516, DOI:10.1021/acsami.0c06516.

[27] S. Chatterjee, K. Sengupta, *Direct Methanol Fuel Cell Technol.*, Elsevier **2020**, pp. 135–176, DOI:10.1016/B978-0-12-819158-3.00006-9.

[28] K. Herkendell, *Catalysts* **2021**, *11*, 278, DOI:10.3390/catal11020278.

[29] S. Schlager, L. M. Dumitru, M. Haberbauer, A. Fuchsbauer, H. Neugebauer, D. Hiemetsberger, A. Wagner, E. Portenkirchner, N. S. Sariciftci, *ChemSusChem* **2016**, *9*, 631–635, DOI:10.1002/cssc.201501496.

[30] H. Seelajaroen, S. Spiess, M. Haberbauer, M. M. Hassel, A. Aljabour, S. Thallner, G. M. Guebitz, N. S. Sariciftci, *Sustain. Energy Fuels* **2020**, *4*, 4238–4248, DOI:10.1039/D0SE00770F.

[31] P. Joshi, R. Mishra, R. J. Narayan, *Curr. Opin. Biomed. Eng.* **2021**, *18*, 100274, DOI:10.1016/j.cobme.2021.100274.

[32] I. Dierking, *C* **2020**, *6*, 80, DOI:10.3390/c6040080.

[33] R. Ding, Y. Huang, G. Li, Q. Liao, T. Wei, Y. Liu, Y. Huang, H. He, *Front. Chem.* **2020**, *8*, 1–20, DOI:10.3389/fchem.2020.607504.

[34] Y. Chen, X. Guo, A. Liu, H. Zhu, T. Ma, *Sustain. Energy Fuels* **2021**, *5*, 3017–3038, DOI:10.1039/D1SE00265 A.

[35] G. S. dos Reis, H. P. de Oliveira, S. H. Larsson, M. Thyrel, E. Claudio Lima, *Nanomaterials* **2021**, *11*, 424, DOI:10.3390/nano11020424.

[36] P. Li, T. Shang, X. Dong, H. Li, Y. Tao, Q. Yang, *Small* **2021**, *2007548*, 2007548, DOI:10.1002/smll.202007548.

[37] D. Werner, D. H. Apaydin, E. Portenkirchner, *Batteries & Supercaps* **2018**, *1*, 160–168, DOI:10.1002/batt.201800057.

[38] D. Werner, D. H. Apaydin, D. Wielend, K. Geistlinger, W. D. Saputri, U. J. Griesser, E. Dražević, T. S. Hofer, E. Portenkirchner, *J. Phys. Chem. C* **2021**, *125*, 3745–3757, DOI:10.1021/acs.jpcc.0c10778.

[39] S. Liebl, D. Werner, D. H. Apaydin, D. Wielend, K. Geistlinger, E. Portenkirchner, *Chem. A Eur. J.* **2020**, *26*, 17559–17566, DOI:10.1002/chem.202003624.

[40] B. Wang, X. Gao, L. Xu, K. Zou, P. Cai, X. Deng, L. Yang, H. Hou, G. Zou, X. Ji, *Batteries & Supercaps* **2021**, *4*, 538–553, DOI:10.1002/batt.202000291.

[41] S. Günes, H. Neugebauer, N. S. Sariciftci, *Chem. Rev.* **2007**, *107*, 1324–1338, DOI:10.1021/cr050149z.

[42] L. Duan, A. Uddin, *Adv. Sci.* **2020**, *7*, 1903259, DOI:10.1002/advs.201903259.

[43] Z. A. Lamport, H. F. Haneef, S. Anand, M. Waldrip, O. D. Jurchescu, *J. Appl. Phys.* **2018**, *124*, 071101, DOI:10.1063/1.5042255.

[44] S.-J. Zou, Y. Shen, F.-M. Xie, J.-D. Chen, Y.-Q. Li, J.-X. Tang, *Mater. Chem. Front.* **2020**, *4*, 788–820, DOI:10.1039/C9QM00716D.

[45] D. H. Apaydin, S. Schlager, E. Portenkirchner, N. S. Sariciftci, *ChemPhysChem* **2017**, *18*, 3094–3116, DOI:10.1002/cphc.201700148.

[46] L. Yao, A. Rahmanudin, N. Guijarro, K. Sivula, *Adv. Energy Mater.* **2018**, *8*, 1802585, DOI:10.1002/aenm.201802585.

[47] W. Zhou, G. Liu, B. Yang, Q. Ji, W. Xiang, H. He, Z. Xu, C. Qi, S. Li, S. Yang, et al., *Sci. Total Environ.* **2021**, *780*, 146483, DOI:10.1016/j.scitotenv.2021.146483.

[48] X. Han, Q. Zhang, H. Liu, J. Sun, *J. Electron. Mater.* **2019**, *48*, 5055–5061, DOI:10.1007/s11664-019-07308-1.

[49] A. Iordache, V. Delhorbe, M. Bardet, L. Dubois, T. Gutel, L. Picard, *ACS Appl. Mater. Interfaces* **2016**, *8*, 22762–22767, DOI:10.1021/acsami.6b07591.

[50] M. Armand, S. Grugeon, H. Vezin, S. Laruelle, P. Ribière, P. Poizot, J.-M. Tarascon, *Nat. Mater.* **2009**, *8*, 120–125, DOI:10.1038/nmat2372.

[51] G. Hernández, N. Casado, A. M. Zamarayeva, J. K. Duey, M. Armand, A. C. Arias, D. Mecerreyes, *ACS Appl. Energ. Mater.* **2018**, *1*, 7199–7205, DOI:10.1021/acsaem.8b01663.

[52] D. Wu, G. Zhang, D. Lu, L. Ma, Z. Xu, X. Xi, R. Liu, P. Liu, Y. Su, *J. Mater. Chem. A* **2018**, *6*, 13613–13618, DOI:10.1039/C8TA03186 J.

[53] W. Deng, Y. Shen, J. Qian, Y. Cao, H. Yang, *ACS Appl. Mater. Interfaces* **2015**, *7*, 21095–21099, DOI:10.1021/acsami.5b04325.

[54] X. Zhang, X. Lu, Y. Shen, J. Han, L. Yuan, L. Gong, Z. Xu, X. Bai, M. Wei, Y. Tong, et al., *Chem. Commun. (Camb.)* **2011**, *47*, 5804–6, DOI:10.1039/c1cc10389j.

[55] Y. Liu, F. Harnisch, K. Fricke, U. Schröder, V. Climent, J. M. Feliu, *Biosens. Bioelectron.* **2010**, *25*, 2167–2171, DOI:10.1016/j.bios.2010.01.016.

[56] S. ur Rahman, P. Röse, M. Surati, A. U. H. A. Shah, U. Krewer, S. Bilal, *Polymers (Basel).* **2020**, *12*, 2705, DOI:10.3390/polym12112705.

[57] W. Honggowiranto, E. Kartini, A. Sudjatno, *Iop. Conf. Ser. Mater. Sci. Eng.* **2020**, *924*, 012036, DOI:10.1088/1757-899X/924/1/012036.

[58] Y. Purwamargapratala, Sudaryanto, F. Akbar, *J. Phys. Conf. Ser.* **2020**, *1436*, 012029, DOI:10.1088/1742-6596/1436/1/012029.

[59] B. J. Landi, C. D. Cress, R. P. Raffaelle, *J. Mater. Res.* **2010**, *25*, 1636–1644, DOI:10.1557/JMR.2010.0209.

[60] R. Muzyka, S. Drewniak, T. Pustelny, M. Chrubasik, G. Gryglewicz, *Materials (Basel).* **2018**, *11*, 15–17, DOI:10.3390/ma11071050.

[61] A. Merlen, J. G. Buijnsters, C. Pardanaud, *Coatings.* **2017**, *7*, 153, DOI:10.3390/coatings7100153.

[62] L. Bokobza, J.-L. Bruneel, M. Couzi, *C* **2015**, *1*, 77–94, DOI:10.3390/c1010077.

[63] A. C. Ferrari, D. M. Basko, *Nat. Nanotechnol.* **2013**, *8*, 235–246, DOI:10.1038/nnano.2013.46.

[64] A. C. Ferrari, *Solid State Commun.* **2007**, *143*, 47–57, DOI:10.1016/j.ssc.2007.03.052.

[65] A. Ferrari, J. Robertson, *Phys. Rev. B: Condens. Matter Mater. Phys.* **2000**, *61*, 14095–14107, DOI:10.1103/PhysRevB.61.14095.

[66] M. A. Pimenta, G. Dresselhaus, M. S. Dresselhaus, L. G. Cançado, A. Jorio, R. Saito, *Phys. Chem. Chem. Phys.* **2007**, *9*, 1276–1291, DOI:10.1039/b613962k.

[67] L. Malard, M. Pimenta, G. Dresselhaus, M. Dresselhaus, *Phys. Rep.* **2009**, *473*, 51–87, DOI:10.1016/j.physrep.2009.02.003.

[68] A. K. Singh, N. Yasri, K. Karan, E. P. L. Roberts, *ACS Appl. Energ. Mater.* **2019**, *2*, 21, DOI:10.1021/acsaem.9b00180.

[69] C. Chen, Y. Wen, X. Hu, X. Ji, M. Yan, L. Mai, P. Hu, B. Shan, Y. Huang, *Nat. Commun.* **2015**, *6*, 6929, DOI:10.1038/ncomms7929.

[70] J. Heinze, *Angew. Chem.* **1984**, *11*, 823–916.

[71] A. R. C. Bredar, A. L. Chown, A. R. Burton, B. H. Farnum, *ACS Appl. Energ. Mater.* **2020**, *3*, 66–98, DOI:10.1021/acsaem.9b01965.

[72] R. Memming, *Solid State Ionics* **1997**, *94*, 131–140, DOI:10.1016/S0167-2738(96)00506-1.

[73] C. Choi, D. S. Ashby, D. M. Butts, R. H. DeBlock, Q. Wei, J. Lau, B. Dunn, *Nat. Rev. Mater.* **2020**, *5*, 5–19, DOI:10.1038/s41578-019-0142-z.

[74] E. Laviron, L. Roullier, C. Degrand, *J. Electroanal. Chem.* **1980**, *112*, 11–23, DOI:10.1016/S0022-0728(80)80003-9.

[75] M. J. Honeychurch, G. A. Rechnitz, *Electroanalysis* **1998**, *10*, 285–293, DOI:10.1002/(SICI)1521-4109(199804)10:5<285::AID-ELAN285>3.0.CO;2-B.

[76] H. Daifuku, K. Aoki, K. Tokuda, H. Matsuda, *J. Electroanal. Chem.* **1985**, *183*, 1–26, DOI:10.1016/0368-1874(85)85478-2.

[77] V. Augustyn, J. Come, M. A. Lowe, J. W. Kim, P.-L. Taberna, S. H. Tolbert, H. D. Abruña, P. Simon, B. Dunn, *Nat. Mater.* **2013**, *12*, 518–522, DOI:10.1038/nmat3601.

[78] T. Brousse, D. Bélanger, J. W. Long, *J. Electrochem. Soc.* **2015**, *162*, A5185–A5189, DOI:10.1149/2.0201505jes.

[79] E. Portenkirchner, D. Werner, S. Liebl, D. Stock, A. Auer, J. Kunze-Liebhäuser, *ACS Appl. Energ. Mater.* **2018**, *1*, 6646–6653, DOI:10.1021/acsaem.8b01712.

[80] H. Lindström, S. Södergren, A. Solbrand, H. Rensmo, J. Hjelm, A. Hagfeldt, S.-E. Lindquist, *J. Phys. Chem. B* **1997**, *101*, 7717–7722, DOI:10.1021/jp970490q.

[81] J. Wang, J. Polleux, J. Lim, B. Dunn, *J. Phys. Chem. C* **2007**, *111*, 14925–14931, DOI:10.1021/jp074464w.

[82] M. Yoshio, R. J. Brodd, A. Kozawa, Eds., *Lithium-Ion Batteries*, Springer New York, New York, NY **2009**, DOI:10.1007/978-0-387-34445-4.

[83] F. Fabregat-Santiago, G. Garcia-Belmonte, I. Mora-Seró, J. Bisquert, *Phys. Chem. Chem. Phys.* **2011**, *13*, 9083, DOI:10.1039/c0cp02249 g.

[84] A. Sacco, *Renewable Sustainable Energy Rev.* **2017**, *79*, 814–829, DOI:10.1016/j.rser.2017.05.159.

[85] G. Garcia-Belmonte, P. P. Boix, J. Bisquert, M. Sessolo, H. J. Bolink, *Sol. Energy Mater. Sol. Cells* **2010**, *94*, 366–375, DOI:10.1016/j.solmat.2009.10.015.

[86] G. del Pozo, B. Arredondo, B. Romero, G. Susanna, F. Brunetti, *Sol. Energy* **2017**, *144*, 105–110, DOI:10.1016/j.solener.2017.01.003.

[87] J. Brumbarov, J. P. Vivek, S. Leonardi, C. Valero-Vidal, E. Portenkirchner, J. Kunze-Liebhäuser, *J. Mater. Chem. A* **2015**, *3*, 16469–16477, DOI:10.1039/C5TA03621F.

[88] D. Werner, C. Griesser, D. Stock, U. J. Griesser, J. Kunze-Liebhäuser, E. Portenkirchner, *ACS Appl. Energ. Mater.* **2020**, *3*, DOI 10.1021/acsaem.9b02541, DOI:10.1021/acsaem.9b02541.

[89] A. Auer, D. Steiner, E. Portenkirchner, J. Kunze-Liebhäuser, *ACS Appl. Energ. Mater.* **2018**, *1*, 1924–1929, DOI:10.1021/acsaem.7b00319.

[90] T. Osaka, D. Mukoyama, H. Nara, *J. Electrochem. Soc.* **2015**, *162*, A2529–A2537, DOI:10.1149/2.0141514jes.

[91] R. Ruffo, S. S. Hong, C. K. Chan, R. a Huggins, Y. Cui, *J. Phys. Chem. C* **2009**, *113*, 11390–11398, DOI:10.1021/jp901594 g.

[92] D. H. Apaydin, M. Gora, E. Portenkirchner, K. T. Oppelt, H. Neugebauer, M. Jakesova, E. D. Głowacki, J. Kunze-Liebhäuser, M. Zagorska, J. Mieczkowski, et al., *ACS Appl. Mater. Interfaces* **2017**, *9*, 12919–12923, DOI:10.1021/acsami.7b01875.

[93] D. H. Apaydin, E. Portenkirchner, P. Jintanalert, M. Strauss, J. Luangchaiyaporn, N. S. Sariciftci, P. Thamyongkit, *Sustain. Energy Fuels* **2018**, *2*, 2747–2753, DOI:10.1039/C8SE00422F.

[94] D. H. Apaydin, H. Seelajaroen, O. Pengsakul, P. Thamyongkit, N. S. Sariciftci, J. Kunze-Liebhäuser, E. Portenkirchner, *ChemCatChem* **2018**, *10*, 1793–1797, DOI:10.1002/cctc.201702055.

[95] L. Bertoluzzi, P. Lopez-Varo, J. A. Jiménez Tejada, J. Bisquert, *J. Mater. Chem. A* **2016**, *4*, 2873–2879, DOI:10.1039/C5TA03210E.

[96] A. J. Bard, L. R. Faulkner, *Electrochemical Methods: Fundamentals and Applications*, WILEY-VCH **2000**.

[97] E. Barsoukov, J. R. Macdonald, Eds., *Impedance Spectroscopy: Theory, Experiment, and Applications*, John Wiley & Sons, Inc., New Jersey **2005**.

[98] A. J. Bard, L. R. Faulkner, *ELECTROCHEMICAL METHODS: Fundamentals and Applications*, John Wiley & Sons Ltd, **2001**.

[99] J. Landesfeind, J. Hattendorff, A. Ehrl, W. A. Wall, H. A. Gasteiger, *J. Electrochem. Soc.* **2016**, *163*, A1373–A1387, DOI:10.1149/2.1141607jes.

[100] Y. Itou, N. Ogihara, S. Kawauchi, *J. Phys. Chem. C* **2020**, *124*, 5559–5564, DOI:10.1021/acs.jpcc.9b11929.

[101] M. Eikerling, A. Kornyshev, *J. Electroanal. Chem.* **1999**, *475*, 107–123, DOI:10.1016/S0022-0728(99)00335-6.

[102] N. Ogihara, S. Kawauchi, C. Okuda, Y. Itou, Y. Takeuchi, Y. Ukyo, *J. Electrochem. Soc.* **2012**, *159*, A1034–A1039, DOI:10.1149/2.057207jes.

[103] N. Ogihara, Y. Itou, T. Sasaki, Y. Takeuchi, *J. Phys. Chem. C* **2015**, *119*, 4612–4619, DOI:10.1021/jp512564 f.

[104] N. C. Walton, J. Wincott, P. Fairley, *Peak Fitting with CasaXPS: A Casa Pocket Book*, Accolyte Science, Knutsford, UK **2010**.

Manuscript received: July 28, 2021
Revised manuscript received: September 14, 2021
Version of record online: October 7, 2021